

Multiple reentrance transitions in exclusion process with finite reservoirTamizhazhagan S  and Atul Kumar Verma **Department of Mathematics, National Institute of Technology, Tiruchirappalli 620 015, Tamilnadu, India*

(Received 28 October 2022; accepted 17 April 2023; published 28 April 2023)

The proposed study is motivated by the scenario of two-way vehicular traffic. We consider a totally asymmetric simple exclusion process in the presence of a finite reservoir along with the particle attachment, detachment, and lane-switching phenomena. The various system properties in terms of phase diagrams, density profiles, phase transitions, finite size effect, and shock position are analyzed, considering the available number of particles in the system and different values of coupling rate, by employing the generalized mean-field theory and the obtained results are detected to be a good match with the Monte Carlo simulation outcomes. It is discovered that the finite resources significantly affect the phase diagram for different coupling rate values, which leads to nonmonotonic changes in the number of phases in the phase plane for comparatively minor lane-changing rates and produces various exciting features. We calculate the critical value of the total number of particles in the system at which the multiple phases in the phase diagram appear or disappear. The competition between the limited particles, bidirectional motion, Langmuir kinetics, and particle lane-shifting behavior yields unanticipated and unique mixed phases, including the double shock phase, multiple reentrance and bulk-induced phase transitions, and phase segregation of the single shock phase.

DOI: [10.1103/PhysRevE.107.044133](https://doi.org/10.1103/PhysRevE.107.044133)**I. INTRODUCTION**

In real life, transport is one of the most crucial aspects of natural and man-made nonequilibrium systems. Understanding the collective behavior of such systems is very challenging due to a continuous supply of internal or external energy resulting in nonzero current in the system, even in the stationary state. In the last few years, a paradigmatic model, the totally asymmetric simple exclusion process (TASEP), first introduced in 1968 by Macdonald and Gibbs to understand the kinetics of biopolymerization [1], has been exploited to explain the characteristics of nonequilibrium stationary properties of the various kinds of transport systems. In the TASEP, particles are distributed on a one-dimensional discrete lattice concerning the hard-core volume constraint due to which, at any time step, a lattice site can accommodate a maximum of one particle. Besides, according to the predefined dynamical rates, particles enter and exit from the first and last sites of the lattice, respectively, and in bulk sites (except the boundary sites) of the lattice, particles hop only in one direction. In past decades, this family of models has been applied in various branches of science, including the nature of ant trails, intracellular transport, vehicular traffic, protein synthesis, and gel electrophoresis [2–7]. Even though the model looks simple, it produces extraordinarily complex features from nonequilibrium physics such as phase separation, boundary-induced phase transitions, symmetry breaking, phase separation, and bulk-induced phase transitions [8–13]. Besides, in literature, the TASEP model has been studied with the consideration of open and closed

systems incorporating the disordered hopping rate [14–16]. Scientific evidence [17] from molecular biology assures that, during the intracellular transport process, molecular motors can join or leave the bulk sites of the microtubule, which inspired the researchers to take the TASEP study to the next level. Using this scenario, the TASEP model has been investigated by employing nonconserving dynamics, namely, Langmuir kinetics (LK), in which a particle can either attach to or detach from the bulk sites of the lattice. It is also more appropriate to model the vehicular traffic phenomena where the vehicles either join or leave the main road by utilizing the branch roads. Apart from the application point of view, the implementation of LK dynamics on the TASEP affects the nature of the system significantly due to the interplay of particle conservation and nonconservation dynamics leading to various features and crucial topological changes in the phase diagram [9,18,19].

Besides, researchers have started investigations on the TASEP model involving multiple channels, motivated by the existing real-life example of intracellular transport processes in which the motor proteins can hop from one microfilament to another to complete the work earlier. Likewise, in vehicular traffic, a vehicle can interchange lanes according to its better motility. So, incorporated with these scenarios, the multilane TASEP model has been scrutinized with different kinds of coupling rules where particles can move from one lane to another according to their travel preference [20–22]. Moreover, to make these multichannel TASEP studies more realistic, the scientist also incorporates the LK dynamics on lanes. It is noticed that the association of LK rules leads to the existence of more steady-state phases, which dramatically affects the phase diagram's topology, as reported in the literature [8,23,24].

*atulv085@gmail.com

In real life, most transport processes exhibit the participation of a finite number of particles incorporating both the system and its surroundings. For example, in vehicular traffic, protein synthesis, and molecular motors transport, the number of vehicles, ribosomes, and kinesins moving along roads, mRNA, and microtubules are far from infinite, respectively [25,26]. Due to the limited number of particles in this system, the entry and attachment rates rely on the available resources in the environment. In all the aforementioned studies on standard TASEPs, the incidence of particle absorption on the lattice depends on the predefined fixed rates [8,23,24]. To incorporate the impact of finite resources, a few studies have recently been conducted on single- and multilane TASEPs with finite reservoir [27–33] in which entry rate depends on reservoir density. Recently, the limited resources on the TASEP model have been considered in which particle entry and exit rates depend on the number of particles in the reservoir [34]. In this direction, the comprehensive study on limited resources on the one-lane TASEP has been examined in the presence of LK, where both attachment and detachment rates rely on the available number of particles in the reservoir [35]. With the help of mean-field theory (MFT) and Monte Carlo simulation (MCS), the stationary properties of the system have been scrutinized through the density profiles, phase planes, and shock positions for the various magnitudes of LK and filling factors. It has been reported that incorporating dynamic LK rates simplifies the complexity of the phase diagram in comparison to the model without LK [34].

It is important to note that past studies based on finite reservoirs focus on unidirectional movement; however, in nature, various systems, including traffic flow and intracellular transport, involve multiple lanes with particle movement in opposite directions. So far, there is no study on a bidirectional TASEP with limited resources incorporated with LK and coupling dynamics. From the vehicular traffic point of view, it is evident that only a finite number of vehicles travel on the road daily. To stimulate a more realistic vehicular traffic model, in this study, we consider a symmetrically coupled bidirectional two-lane TASEP with the affiliation of limited resources and LK dynamics. Similarly, in a biological cell, molecular motors can travel along multiple protofilaments in opposite directions, switch their paths, and attach to or detach from the microtubule [36,37]. Moreover, the number of molecular motors participating in the transport processes is far from infinite [26], which is usually ignored while developing a mathematical model based on motor proteins. Motivated by all these observations and to mimic the intracellular and vehicular transport comparatively more realistically, in this study, we develop a minimal model to understand the stationary properties of such complex processes with a finite reservoir. We also aim to observe the impact of limited resources on the system dynamics in the presence of LK and varied coupling processes.

In Sec. II, we explain the model and its dynamical rules in detail. In Sec. III, we show the master equation of the proposed model, and Sec. IV is used to discuss the obtained results and summarize the features of the distinguishable finding of our proposed study. Finally, in Sec. V, we briefly

discuss the vital outlook characterization of the proposed model.

II. MODEL DESCRIPTION

We simulate the system dynamics by considering the two parallel one-dimensional discrete lattices with L sites named lane A and lane B. Lattice sites are labeled as $i = 1, 2, \dots, L$, in which both ends of lattices are connected with a reservoir R accommodating a finite number of particles, $N_R(t)$, at any time t which do not have any internal dynamics. The system setup can be considered as two open lattices with $L + 1$ sites, in which the site $i = 0$ is treated as a reservoir R that can be occupied by more than one particle. Further, motivated by the real-life example of a finite pool of transport processes, we construct a model in such a way that the lanes and reservoir compete only through the constant number of particles, N_T , which is the sum of the number of particles in the reservoir and particles in lanes at any time t . The directive motion of the particles varies depending on their residence lanes. A particle on lane A (B) always travels from the left (right) to the right (left) direction except for the time of lane-switching phenomena, as displayed in Fig. 1. The occupation state of sites of the lattices follows the excluded volume constraint such that each site is either empty or occupied by rightly one particle. Therefore, the state of the site is represented by a Bernoulli variable $\tau_{i,j}$ ($j = A, B$), which takes the value 0 (1) if the site is empty (occupied). The system obeys the random sequential update rule in which, at each time step, a site (i, j) is chosen randomly, and it gets updated according to the following possible dynamical rules of the system.

(1) *At the entrance site of the lanes:* A particle from a reservoir can hop to the first (last) site of lane A (B) with rate α_{eff} depending upon the reservoir density ($N_R(t)/N_T$) when the site is vacant.

(2) *At the bulk sites of the lanes:* If the site (i, j) is empty, a particle can attach to the site from a reservoir with the rate $\omega_{a\text{eff}}$ depending upon the reservoir density ($N_R(t)/N_T$). In case it is nonempty, a particle first tries to detach from the site to the reservoir with a rate ω_d . If it fails to detach from the site, then it jumps to the onward site (depending on the motion of the lane) of the same lane with the unit hopping rate. A particle attempt that fails on these two events then shifts to the analogous site on the opposite lane for the rate ω only if the targeted site is empty.

(3) *At the exit site of the lanes:* A particle can exit from the last (first) site of lane A (B) to the reservoir with a rate β .

It is important to note that, except for the direction of the particle motility, all other dynamical rules are the same in both lanes. Besides, there is no interaction between lanes at boundaries.

Since the number of particles in the system is conserved due to its closed infrastructure, the number of particles in the system remains constant at any instant of time t ; we have

$$N_T = N_R(t) + N_A(t) + N_B(t). \quad (1)$$

Here the variables $N_A(t)$ and $N_B(t)$ indicate the total number of particles in lane A and lane B at time t with $0 \leq N_A(t), N_B(t) \leq L$ and $N_R(t)$ denotes the number

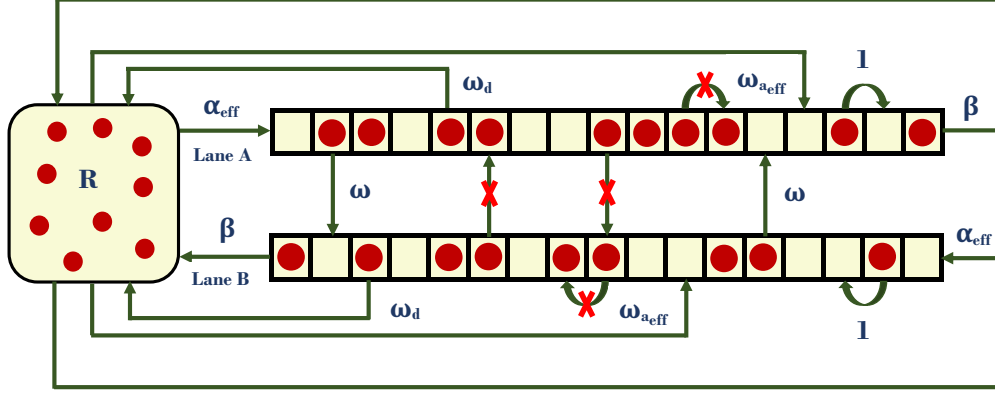


FIG. 1. Model for symmetrically coupled bidirectional two-lane TASEP with Langmuir kinetics and finite supply of particles. The arrows (crossed arrows) indicate the allowed (forbidden) particle transitions. The variable names near the arrows denote the transition rate of the corresponding dynamics, where R represents the finite pool of the reservoir.

of particles in the reservoir R at time t . Therefore, at each time, the effective entry and attachment rate depends on the magnitude of N_R ; along with this observation, the effective entry and attachment rates are defined as follows:

$$\alpha_{\text{eff}} = \alpha f(N_R), \quad (2)$$

$$\omega_{a,\text{eff}} = \omega_a f(N_R), \quad (3)$$

where the function $f(\cdot)$ satisfies the conditions such that $f(0) = 0$ and $f(N_T) = 1$. Physically it is understood that the effective entry rate is zero when there is no particle in the reservoir which signifies the condition $f(0) = 0$. Further, for the infinite reservoir case $N_R(t) \rightarrow N_T$ which implies that $f(N_R(t)) \rightarrow 1$. From this, it is clear that effective entry is the same as the intrinsic entry rate when the reservoir acts as an infinite reservoir. In this way, the function is characterized as follows:

$$f(N_R(t)) = \frac{N_R(t)}{N_T}.$$

Note that the proposed model converges to a standard symmetrically coupled bidirectional two-lane TASEP when $N_R \approx N_T$ for $N_T \rightarrow \infty$ [38].

III. MEAN-FIELD EQUATIONS

The governing densities of bulk sites ($1 < i < L$) of the lane (j) by employing the master equations can be described as follows:

$$\begin{aligned} \frac{d\langle \tau_{i,A} \rangle}{dt} &= \langle \tau_{i-1,A}(1 - \tau_{i,A}) \rangle - \langle \tau_{i,A}(1 - \tau_{i+1,A}) \rangle \\ &+ \omega_{a,\text{eff}} \langle 1 - \tau_{i,A} \rangle - \omega_d \langle \tau_{i,A} \rangle - \omega \langle \tau_{i,A} \tau_{i+1,A}(1 - \tau_{i,B}) \rangle \\ &+ \omega \langle \tau_{i,B} \tau_{i-1,B}(1 - \tau_{i,A}) \rangle, \end{aligned} \quad (4)$$

$$\begin{aligned} \frac{d\langle \tau_{i,B} \rangle}{dt} &= \langle \tau_{i+1,B}(1 - \tau_{i,B}) \rangle - \langle \tau_{i,B}(1 - \tau_{i-1,B}) \rangle \\ &+ \omega_{a,\text{eff}} \langle 1 - \tau_{i,B} \rangle - \omega_d \langle \tau_{i,B} \rangle + \omega \langle \tau_{i,A} \tau_{i+1,A}(1 - \tau_{i,B}) \rangle \\ &- \omega \langle \tau_{i,B} \tau_{i-1,B}(1 - \tau_{i,A}) \rangle, \end{aligned} \quad (5)$$

where the notation $\langle \dots \rangle$ denotes the statistical average. The positive and negative terms on the right-hand sides of the equations correspond to the gain and loss of particles on the lane concerning the possibility of dynamical rules of hopping, LK, and lane-shifting events.

Similarly, at boundary sites ($i = 1, L$) of the lanes, the densities are calculated as follows:

$$\frac{d\langle \tau_{1,A} \rangle}{dt} = \alpha_{\text{eff}} \langle 1 - \tau_{1,A} \rangle - \langle \tau_{1,A}(1 - \tau_{2,A}) \rangle, \quad (6)$$

$$\frac{d\langle \tau_{1,B} \rangle}{dt} = \langle \tau_{2,B}(1 - \tau_{1,B}) \rangle - \beta \langle \tau_{1,B} \rangle, \quad (7)$$

$$\frac{d\langle \tau_{L,A} \rangle}{dt} = \langle \tau_{L-1,A}(1 - \tau_{L,A}) \rangle - \beta \langle \tau_{L,A} \rangle, \quad (8)$$

$$\frac{d\langle \tau_{L,B} \rangle}{dt} = \alpha_{\text{eff}} \langle 1 - \tau_{L,B} \rangle - \langle \tau_{L,B}(1 - \tau_{L-1,B}) \rangle. \quad (9)$$

Using the mean-field theory, we can neglect the correlation between the variables in the above-described equations, i.e., $\langle \tau_{i,j} \tau_{i+1,j} \rangle \approx \langle \tau_{i,j} \rangle \langle \tau_{i+1,j} \rangle$.

To solve the above-discussed equation, for large system size $L \rightarrow \infty$ and small spacing $\epsilon = \frac{1}{L} \rightarrow 0$, the discrete model can be modified into a continuum limit by coarse-graining the discrete lattice with quasicontinuous space variable $x = \frac{i}{L}$ and rescaled time variable $t' = \frac{t}{L}$. To analyze the interplay between the dynamics of LK and lane-changing rules with the system size, we rescale the LK and coupling rates as follows: $\Omega_{a,\text{eff}} = \omega_{a,\text{eff}} L$, $\Omega_d = \omega_d L$, and $\Omega = \omega L$. In the continuum limit, the discrete variable $\langle \tau_{i,j} \rangle$ is replaced with the continuous variable $\rho_{i,j} \in [0, 1]$ and reserving the terms up to second order in the expansion of the Taylor series we get

$$\rho_{i\pm 1,j} = \rho_{i,j} \pm \frac{1}{L} \frac{\partial \rho_{i,j}}{\partial x} + \frac{1}{2L^2} \frac{\partial^2 \rho_{i,j}}{\partial x^2} \pm \mathcal{O}\left(\frac{1}{L^3}\right). \quad (10)$$

The proposed model does not have any kind of spatial inhomogeneity in bulk sites of the lane, so we neglect the subscript i from the derivation of equations. The average density of the

lane at bulk sites evolves as follows:

$$\begin{aligned} \frac{\partial}{\partial t'} \begin{bmatrix} \rho_A \\ \rho_B \end{bmatrix} + \frac{\partial}{\partial x} \begin{bmatrix} -\frac{\epsilon}{2} \frac{\partial \rho_A}{\partial x} + \rho_A(1 - \rho_A) \\ -\frac{\epsilon}{2} \frac{\partial \rho_B}{\partial x} - \rho_B(1 - \rho_B) \end{bmatrix} \\ = \begin{bmatrix} \Omega_{a_{\text{eff}}}(1 - \rho_A) - \Omega_d \rho_A - \Omega \rho_A^2(1 - \rho_B) + \Omega \rho_B^2(1 - \rho_A) \\ \Omega_{a_{\text{eff}}}(1 - \rho_B) - \Omega_d \rho_B + \Omega \rho_A^2(1 - \rho_B) - \Omega \rho_B^2(1 - \rho_A) \end{bmatrix}. \end{aligned} \quad (11)$$

Here, ρ_A and ρ_B represent the densities of lane A and lane B, respectively. The terms featured on the right-hand side of the equation denote the nonconservative dynamics of particle attachment, detachment, and lane-shifting behavior. Under the particular case of LK rates $\Omega_a = \Omega_d$, the steady-state master equation can be modified as

$$\begin{aligned} \frac{\epsilon}{2} \frac{d^2 \rho_A}{dx^2} + (2\rho_A - 1) \frac{d\rho_A}{dx} - \Omega_d(\rho_A(1 + f(N_R)) - f(N_R)) \\ - \Omega \rho_A^2(1 - \rho_B) + \Omega \rho_B^2(1 - \rho_A) = 0, \end{aligned} \quad (12)$$

$$\begin{aligned} \frac{\epsilon}{2} \frac{d^2 \rho_B}{dx^2} + (1 - 2\rho_B) \frac{d\rho_B}{dx} - \Omega_d(\rho_B(1 + f(N_R)) - f(N_R)) \\ + \Omega \rho_A^2(1 - \rho_B) - \Omega \rho_B^2(1 - \rho_A) = 0. \end{aligned} \quad (13)$$

Similarly the boundary conditions reduce to $\rho_A(0) = \rho_B(1) = \alpha_{\text{eff}}$ and $\rho_A(1) = \rho_B(0) = 1 - \beta = \gamma$ (say). Solving the above-mentioned steady-state equations with these boundary conditions is not possible using the numerical techniques because the variables α_{eff} and $\Omega_{a_{\text{eff}}}$ depend upon the value of N_R . To solve the equation system, we use the generalized mean-field theory introduced in past studies [32]. This theory produces the implicit relationship between the variable rates and particle densities. It is clear that the total number of particles in lanes is

$$N_L = N_A + N_B,$$

where N_A and N_B denote the total numbers of particles in lane A and lane B, respectively. In this direction, we can evaluate the total number of particles in lanes at stationary state by using the continuous Riemann sum, and we get

$$N_L = L \left(\int_0^1 \rho_A(x) dx + \int_0^1 \rho_B(x) dx \right). \quad (14)$$

From Eqs. (1) and (14) we attain

$$N_R = N_T - L \left(\int_0^1 \rho_A(x) dx + \int_0^1 \rho_B(x) dx \right). \quad (15)$$

From these equations, the effective rates become

$$\alpha_{\text{eff}} = \alpha \left[1 - \frac{L \left(\int_0^1 \rho_A(x) dx + \int_0^1 \rho_B(x) dx \right)}{N_T} \right], \quad (16)$$

$$\Omega_{a_{\text{eff}}} = \Omega_a \left[1 - \frac{L \left(\int_0^1 \rho_A(x) dx + \int_0^1 \rho_B(x) dx \right)}{N_T} \right]. \quad (17)$$

Using Eqs. (16) and (17), the partial differential equations (12) and (13) becomes

$$\begin{aligned} \frac{\epsilon}{2} \frac{d^2 \rho_A}{dx^2} + (2\rho_A - 1) \frac{d\rho_A}{dx} - \Omega_d \left[\rho_A + (\rho_A - 1) \right. \\ \left. \times \left[1 - \frac{L}{N_T} \left(\int_0^1 \rho_A(x) dx + \int_0^1 \rho_B(x) dx \right) \right] \right] \\ - \Omega \rho_A^2(1 - \rho_B) + \Omega \rho_B^2(1 - \rho_A) = 0, \end{aligned} \quad (18)$$

$$\begin{aligned} \frac{\epsilon}{2} \frac{d^2 \rho_B}{dx^2} + (1 - 2\rho_B) \frac{d\rho_B}{dx} - \Omega_d \left[\rho_B + (\rho_B - 1) \right. \\ \left. \times \left[1 - \frac{L}{N_T} \left(\int_0^1 \rho_A(x) dx + \int_0^1 \rho_B(x) dx \right) \right] \right] \\ + \Omega \rho_A^2(1 - \rho_B) - \Omega \rho_B^2(1 - \rho_A) = 0. \end{aligned} \quad (19)$$

Now the above system of equations can be solved using suitable numerical methods with the boundary conditions $\rho_A(0) = \rho_B(1) = \alpha_{\text{eff}}$ and $\rho_A(1) = \rho_B(0) = \gamma$.

IV. RESULTS AND DISCUSSION

Our main intention is to analyze the effect of limited resources on a bidirectional symmetrically coupled system with LK in the presence of coupling between the lanes. To understand the characteristic of the steady-state properties of a system, we investigate the phase diagrams in the parameter space of (α, γ) for the different values of lane-changing rate and the total number of particles in the system. Moreover, for the sake of a complete understanding of the nature of the system in the presence of a finite pool, we discuss the proposed model by analyzing phase transition, phase separation, finite size effect, and shock dynamics in upcoming sections.

Lanes are distinguishable only through the motion of particles, and, excluding this, other dynamical rules are the same on both lattices; therefore one can infer that the average density profile of one lane is a mirror image of another lane. Therefore, we have mentioned only the stationary state name of lane A rather than denoting both the steady-state names of the lanes throughout this paper. Further, depending on the average particle density of the lanes, they are named as follows: low density ($\rho < 0.5$), high density ($\rho > 0.5$), and maximal current ($\rho \approx 0.5$), which are in the short form labeled as LD, HD, and MC, respectively. In addition, the shock (S) phase indicates the traffic jamming scenario where the sudden jumping rises from low density to the high-density phase and vice versa. Besides, the mixed phases are denoted as X/Y/Z, where X, Y, and Z belong to one of the discussed stationary phases of LD, HD, MC, and S.

A. Phase diagrams

In this section, we present the overall system dynamics in terms of phase diagrams and explain how the adopted coupling rules impact the stationary properties of the proposed model. Before that, we briefly discuss the results of

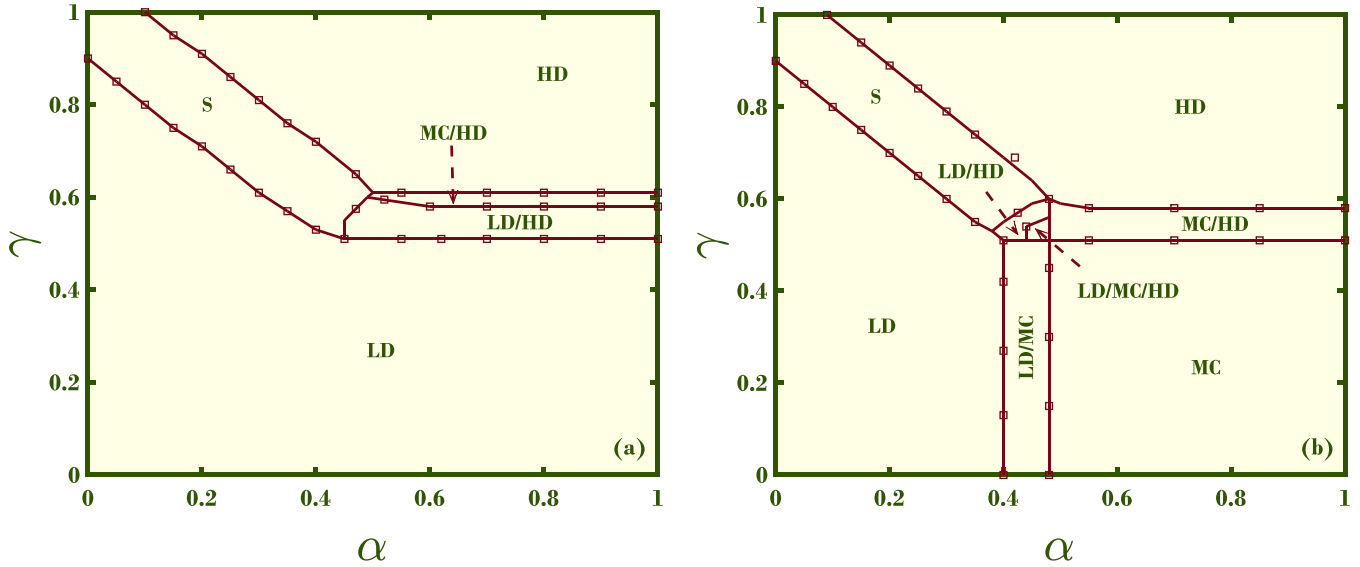


FIG. 2. Phase diagram for single-lane TASEP with LK: (a) $\frac{N_T}{L} = 25$ and (b) $\frac{N_T}{L} \rightarrow \infty$. The parameter values are fixed $\Omega_a = \Omega_d = 0.1$, and $L = 1000$. The solid line (markers) represents the MFT (MCS) results.

the single-lane TASEP model with LK and finite reservoir as follows. For the smaller values of $\frac{N_T}{L}$, the system always remains in the state of LD until $\frac{N_T}{L}$ reaches the value 0.1. At the stage of $\frac{N_T}{L} \approx 0.1$, the shock phase emerges into the phase diagram. Further increasing the available number of particles in the system, the S-phase region starts shrinking due to the appearance of an HD phase in the system when $\frac{N_T}{L}$ reaches the value 2. After $\frac{N_T}{L} > 2$, no significant changes occur in the phase diagram except the phase boundary shifting. When $\frac{N_T}{L}$ reaches the value 12, the phase diagram exhibits the mixed phase LD/HD. In addition, incorporating more particles in the system does not affect the topology of the phase diagram substantially. At $\frac{N_T}{L} \approx 22$, the system experiences the mixed phase MC/HD. Advancing the value of $\frac{N_T}{L}$ from 22, the number of phases in the phase diagram remains the same until it reaches the value 28. Figure 2(a) displays all these phases in the phase diagram for $\frac{N_T}{L} = 25$. At $\frac{N_T}{L} \approx 28$, the phase diagram encompasses three new phases, MC, LD/MC, and LD/MC/HD, owing to the increment of the total number of particles in the system. Beyond the critical value of 28, the system does not experience any new phases; to understand the infrastructure evaluation of the phase plane, we have exhibited the phase diagram for the case of an infinite reservoir in Fig. 2(b).

The previous text discusses the brief results of a single-lane TASEP system with LK and finite resources. Now we analyze how the topology of the phase plane is modified quantitatively and qualitatively for different coupling rate values with the increasing total amount of particles in the system. Besides, we have exhibited some crucial phase diagrams where significant changes emerge in the infrastructure of the phase diagram for distinct values of $\frac{N_T}{L}$ with the lane-changing rate $\Omega = 1$, as displayed in Fig. 3. In addition, using MFT results, we have noticed the critical points for different values of the lane-shifting rate in which the phases get affected qualitatively or quantitatively. Using these critical points, we plotted the

figures, which gives a geometrical understanding of how the phases either increase or decrease or transit into another phase in the phase diagram while crossing each critical value of $\frac{N_T}{L}$. The threshold points are denoted as c_i , d_i , and e_i for the coupling rate $\Omega = 1$, $\Omega = 10$, and $\Omega = 100$, respectively, as shown in Fig. 4. In the figure, the x axis indicates the magnitude of $\frac{N_T}{L}$, and the y axis stands for the total number of phases presented in the phase diagram concerning the particular value of $\frac{N_T}{L}$.

To begin with, we calculate the phase diagrams for specific values of the total number of particles in the system $\frac{N_T}{L} \in [0, \infty)$ displaying the crucial topological changes in the phase diagram due to the appearance or disappearance of the new phases at $\Omega = 1$. It is clear that at $\frac{N_T}{L} = 0$, there is no particle in the system. For comparatively small nonzero values of $\frac{N_T}{L} \approx c_1 \approx 0$, the system experiences only a low-density phase due to the unavailability of many particles for the lanes. While the value of $\frac{N_T}{L}$ reaches the second critical value of $c_2 \approx 0.09$, the single shock phase S emerges into the phase diagram, and further beyond the value of c_2 , the unique double shock phase \tilde{D} arises in the phase diagram at critical point $c_3 \approx 1.2$, which leads to condensing the occupied region of the single shock phase. As a result of this, the double shock region looks like a peninsula around the single shock phase region, as shown in Fig. 3(a). In other words, the single shock phase gets segregated into two portions by the emergence of the double shock phase. Due to the dramatic structure of the shock phase region in the phase space, one can travel through the phase diagram vertically (horizontally) for the increasing values of γ (α) with fixed remaining parameters; the system experiences the S phase two times through the phase transition of $S \rightarrow \tilde{D} \rightarrow S$ [see Fig. 3(a)]. These kinds of phase transitions have been reported in the name of multiple phase transitions or back-and-forth effects or reentrant or reentrance transitions in literature [38–42]. We will go into more detail about reentrance transitions in forthcoming subsections. It is noteworthy to mention that the stationary state of the double

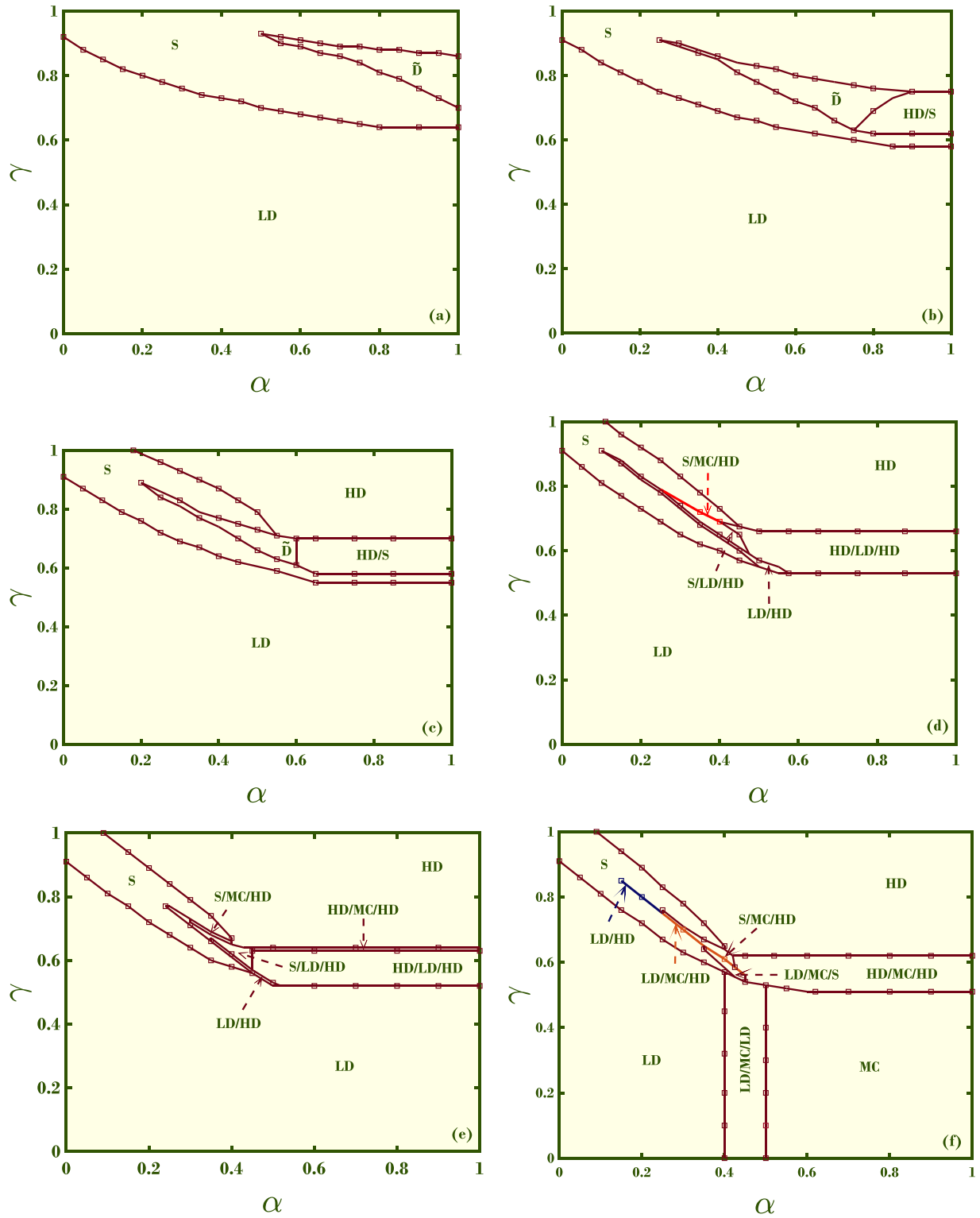


FIG. 3. Phase diagram for (a) $\frac{N_T}{L} = 1.4$, (b) $\frac{N_T}{L} = 2$, (c) $\frac{N_T}{L} = 3.5$, (d) $\frac{N_T}{L} = 9.5$, (e) $\frac{N_T}{L} = 25$, and (f) $\frac{N_T}{L} = 100$. The other parameter values are fixed as $\Omega_a = \Omega_d = 0.1$, $\Omega = 1$ with the system size $L = 1000$. The solid line (markers) indicate results from MFT (MCS).

shock has not been found in past studies of the TASEP model with the incorporation of limited resources [30,32,33,43].

Further increasing the magnitude of $\frac{N_T}{L}$ from c_3 , the new mixed phase HD/S appears at $c_4 \approx 1.5$ as displayed in Fig. 3(b), which leads to phase region shrinkage of \tilde{D} . Physically, it is recognized that an increment in the availability of

particles increases the particle arrivals in the entry site, which affect the double shock phase in such a way that near the left boundary shock transits into high density [see Fig. 6(a)]. Advancing the value of $\frac{N_T}{L}$ from c_4 , the HD phase arises in the stationary phase diagram after crossing the critical point $c_5 \approx 2$, and further enhancing the value of $\frac{N_T}{L}$ from c_5 , the

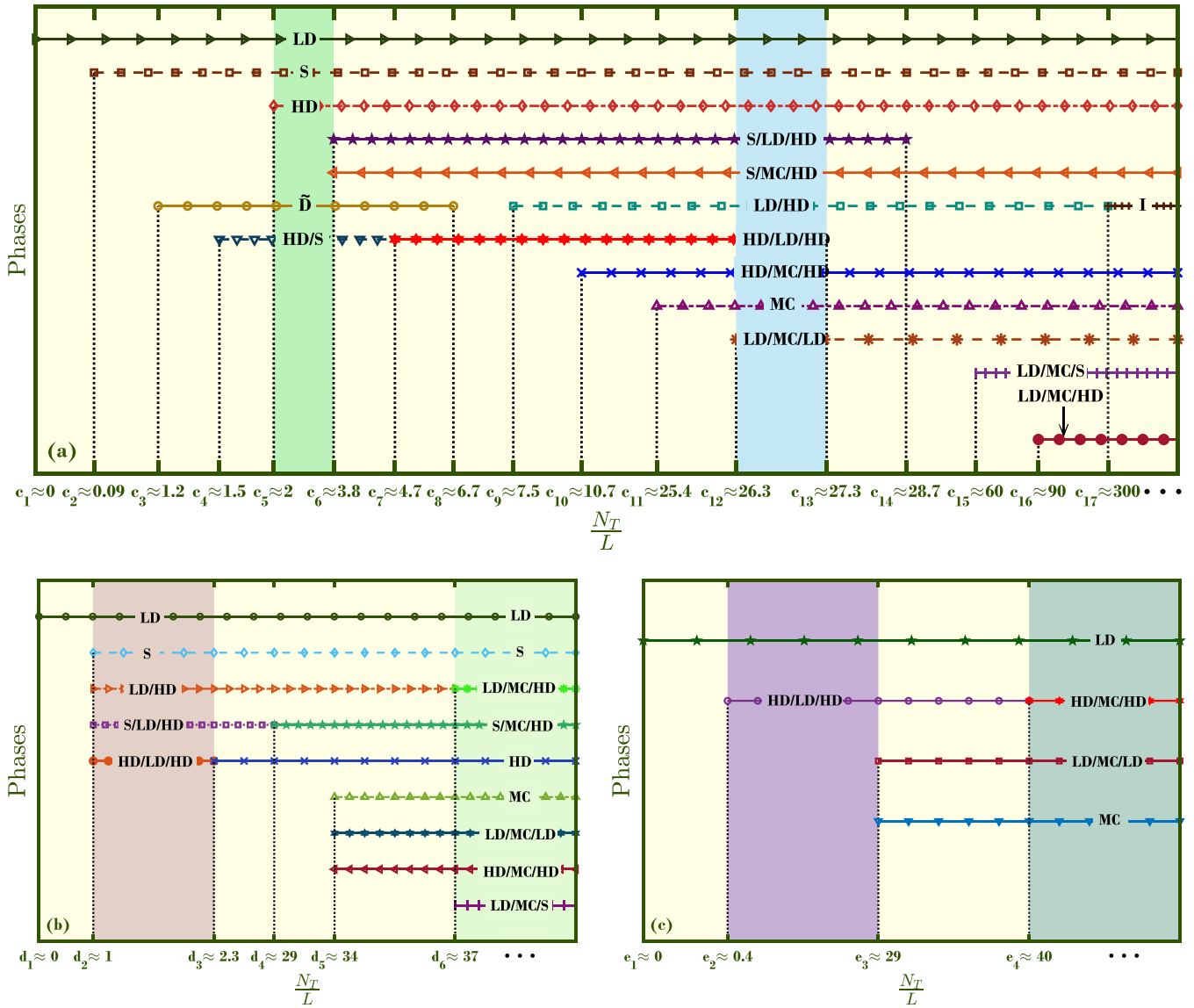


FIG. 4. Phase transitions with $\frac{N_T}{L}$ for $L = 1000$. The attachment and detachment rates are fixed as $\Omega_a = \Omega_d = 0.1$. The coupling rate is kept as (a) $\Omega = 1$, (b) $\Omega = 10$, and (c) $\Omega = 100$. In each figure c_i 's, d_i 's, and e_i 's denote the critical points of their respective case of $\Omega = 1, 10$, and 100 . The y axis denotes the names of all the attained phases in the phase diagram for specific values of $\frac{N_T}{L}$.

phase region of S and \tilde{D} start shrinking owing to the phase expansion of HD/S and the arrival of the HD phase as shown in Fig. 3(c). In this phase diagram, if one can travel through a vertical direction by increasing the value of γ for a specific value of α ; the system undergoes the single shock phase two times [see Fig. 6(b)]. Besides advancing the value of $\frac{N_T}{L}$, the two new kinds of mixed phases, S/LD/HD and S/MC/HD, appear in the phase diagram at the critical value $c_6 \approx 3.8$ due to the transition (relaxation) of double shock for certain ranges of α and γ . While increasing the value of $\frac{N_T}{L}$ from c_6 , the HD/S phase transits into the mixed phase HD/LD/HD when the value of $\frac{N_T}{L}$ reaches the critical $c_7 \approx 4.7$. Beyond the value of c_7 , the system does not observe any new phases up to the value of $\frac{N_T}{L} \approx 6.7$. From this critical point $c_8 \approx 6.7$, the unique phase \tilde{D} disappears and, further expanding the values $\frac{N_T}{L}$, the LD/HD phase appears in the phase diagram

at $c_9 \approx 7.5$ as shown in Fig. 3(d). It is crucial to observe from this phase diagram that the system experiences a reentrance transition of the single shock phase in two ways where, for instance, with a fixed value of $\gamma = 0.83$ and $\gamma = 0.73$, the system goes through the single shock phase two times in such a way that phase transitions from $S \rightarrow LD/HD \rightarrow S$ and $S \rightarrow LD/HD \rightarrow S/LD/HD \rightarrow S/MC/HD \rightarrow S$, respectively, while advancing the value of α . The most attractive ingredient of this reentrance transition is that the system experiences the S phase after over through the three kinds of distinct mixed phases [see Fig. 8(a)], and furthermore, during these reentrance transitions, the intermediate manifested phases are emanated due to bulk-induced phase transitions. It is clear that the system experiences the reentrance transition involving the S phase in two directions; we refer to this as the “multiple reentrance transition” of the single shock phase. It is

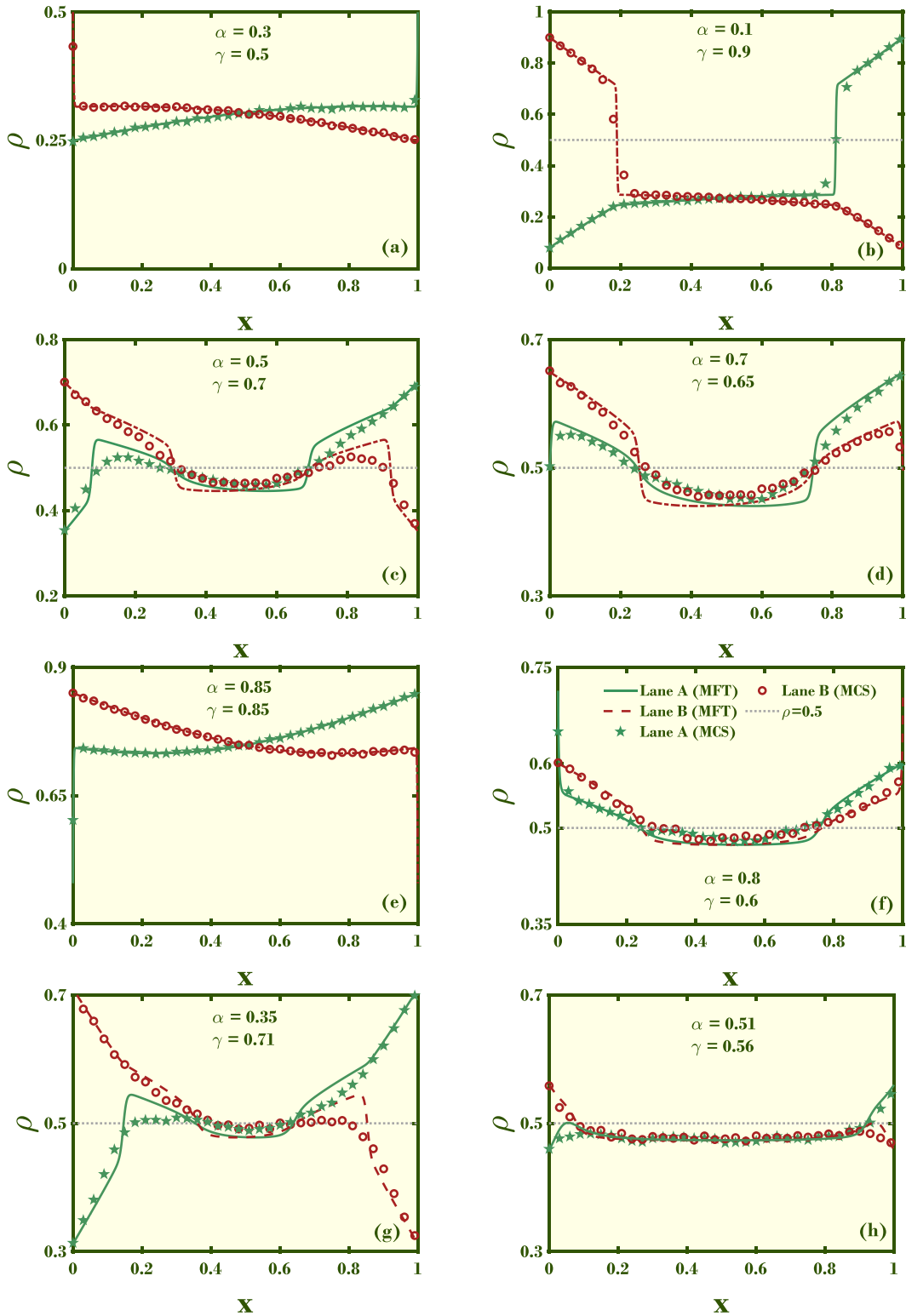


FIG. 5. Density profiles of the lanes for the case of $\frac{N_T}{L} = 3.5$, (a) LD, (b) S, (c) \tilde{D} , (d) HD/S, and (e) HD for $\Omega = 1$; and $\frac{N_T}{L} = 9.5$, (f) HD/LD/HD, (g) S/LD/HD, and (h) LD/HD for $\Omega = 10$. The LK rates are fixed as $\Omega_a = \Omega_d = 0.1$ with the lattice size $L = 1000$.

noteworthy to mention here that this kind of reentrance transition has not been captured in any past studies of the TASEP with the incorporation of the finite reservoir. In addition, while increasing the number of particles in the reservoir beyond the value of c_9 , the mixed phase HD/MC/HD emerges at the

critical point of $c_{10} \approx 10.7$, which results in a diminishing of the phase region of HD/LD/HD as shown in Fig. 3(e). Here also, the system goes through the single shock phase in two different ways in the phase diagram concerning the specific value of α (γ) with increasing value of γ (α) [for a

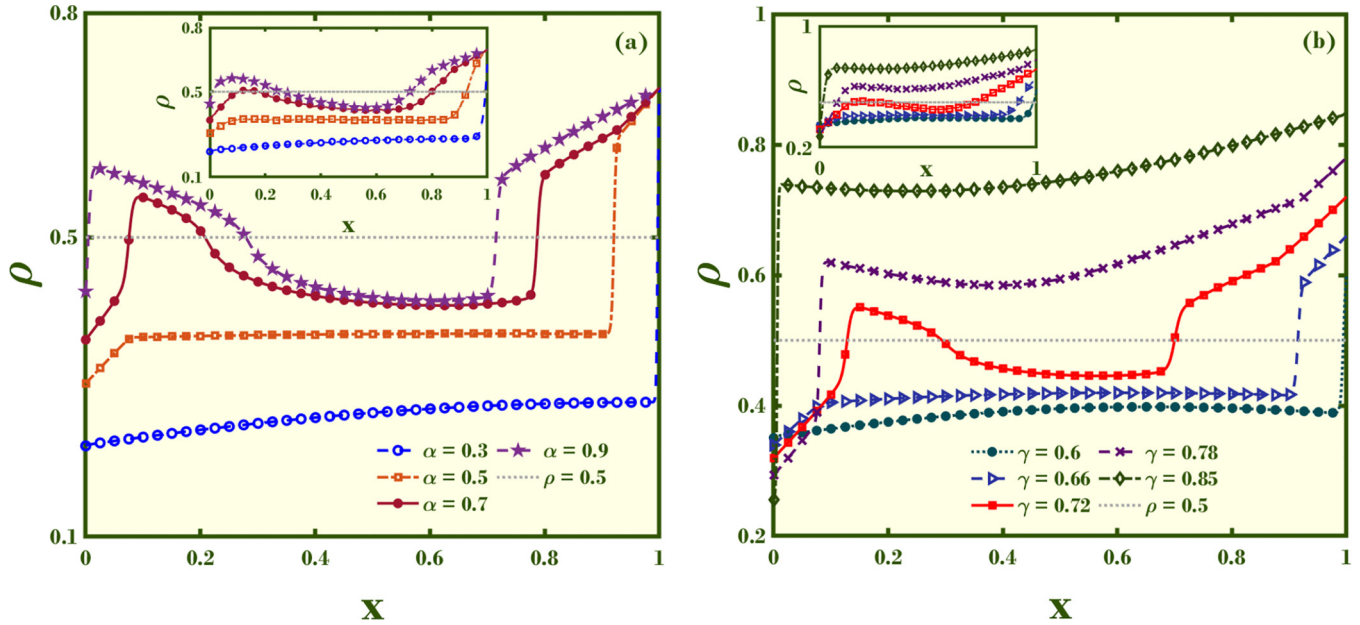


FIG. 6. Phase transitions of lane A from (a) LD → S → \tilde{D} → HD/S for the fixed rate $\gamma = 0.7$ with various entry rate α and $\frac{N_T}{L} = 2$, and (b) LD → S → \tilde{D} → S → HD (reentrance transition of the S phase) for the fixed entry rate $\alpha = 0.45$ with various rates of γ and $\frac{N_T}{L} = 3.5$. The LK and lane-changing rates are fixed as $\Omega_a = \Omega_d = 0.1$ and $\Omega = 1$ with the system size $L = 1000$. The main panel indicates the MFT outcomes, and the insets represent the corresponding MCS results.

better understanding of the unique reentrance transition of the single shock phase, see Fig. 8(b)]. Moreover, on comparison of Fig. 2(a), which shows the phase diagram for single-lane TASEP with LK and finite resources with Fig. 3(e), one can infer how the phase diagram evolved owing to the impact of the coupling rule. We notice that the incorporation of coupling between lanes leads to the vanishing of stationary phases LD/MC and MC and the emergence of mixed phases S/LD/HD, S/MC/HD, HD/LD/HD, and HD/MC/HD, displaying the significant influence of the adopted coupling environment. In addition, increasing the magnitude of $\frac{N_T}{L}$ from c_{10} , the new phases MC and LD/MC/LD start to appear in the phase diagram after crossing the critical points $c_{11} \approx 25.4$ and $c_{12} \approx 26.3$, respectively.

It is important to indicate that the proposed model experiences a greater number of phases in the region of (c_{12}, c_{13}) in which the topology of the phase diagram gets affected substantially, as displayed in Fig. 4(a). Further, increasing the number of particles in the reservoir, at the critical points $c_{13} \approx 27.3$ and $c_{14} \approx 28.7$, the mixed phases HD/LD/HD and S/LD/HD disappear, correspondingly. After c_{14} , the system experiences the same number of phases until it reaches the value $c_{15} \approx 60$. Moreover, LD/MC/S and LD/MC/HD are present in the phase diagram when crossing over the critical points c_{15} and $c_{16} \approx 90$, respectively, as shown in Fig. 3(f). It is worthwhile to observe from the figure that the multiple reentrance transition of the S phase persists in the phase diagram. Beyond the critical point c_{16} , no significant changes are observed in the phase diagram until it reaches the critical point $c_{17} \approx 300$. On the far side of c_{17} , the mixed phase LD/HD starts transiting into the strictly increasing (I) phase, and the phase diagrams become qualitatively the same as the phase diagram of the standard symmetrically coupled bidirectional

TASEP with LK [38]. For $\Omega = 10$, a comparatively small value of $\frac{N_T}{L} \approx d_1 \approx 0$, the system is in the state of LD until it reaches the value 1. At $d_2 \approx 1$, the four distinct phases S, LD/HD, S/LD/HD, and HD/LD/HD appear in the phase diagram. Further, expanding the value of $\frac{N_T}{L}$ from d_2 , among these phases, the HD/LD/HD transits to HD and S/LD/HD transits to S/MC/HD while reaching the critical points $d_3 \approx 2.3$ and $d_4 \approx 29$, subsequently. Beyond the value of $\frac{N_T}{L} > 29$, three different stationary phases, MC, LD/MC/LD, and HD/MC/HD, arise in the phase diagram when it reaches the critical value $d_5 \approx 34$. At this stage, advancing the number of available particles in the system, a new kind of mixed-phase LD/MC/S appears, and the LD/HD phase transits to LD/MC/HD while reaching the critical point of $d_6 \approx 37$. After the value of d_6 , except for the phase boundary shifting, no significant changes are found in the phase diagrams. Also, it is essential to note that the system experiences a greater number of stationary phases when $\frac{N_T}{L} > 37$. It is crucial to mention that after the state of $\frac{N_T}{L} \approx 37$, the phase diagram incorporates exactly nine distinct stationary phases, as shown in Fig. 4(b).

With coupling rate $\Omega = 100$, for a relatively smaller value of $\frac{N_T}{L} \approx e_1 \approx 0$, the topology of the phase diagram is simple and contains only one stationary phase, namely, LD. Further, increasing the total number of particles in the system, a mixed phase HD/LD/HD emerges in the phase diagram at the critical point $e_2 \approx 0.4$. After $\frac{N_T}{L} > 0.4$, the phase diagram does not affect quantitatively until it reaches the point $e_3 \approx 29$. At the critical point of e_3 , the system experiences two kinds of phases, LD/MC/LD and MC. Besides advancing the value of $\frac{N_T}{L}$, no significant changes are observed in the phase diagram until it reaches the critical value of $e_4 \approx 40$. At this stage, e_4 , the mixed phase HD/LD/HD transits to the HD/MC/HD owing to the increment of the number of particles in the

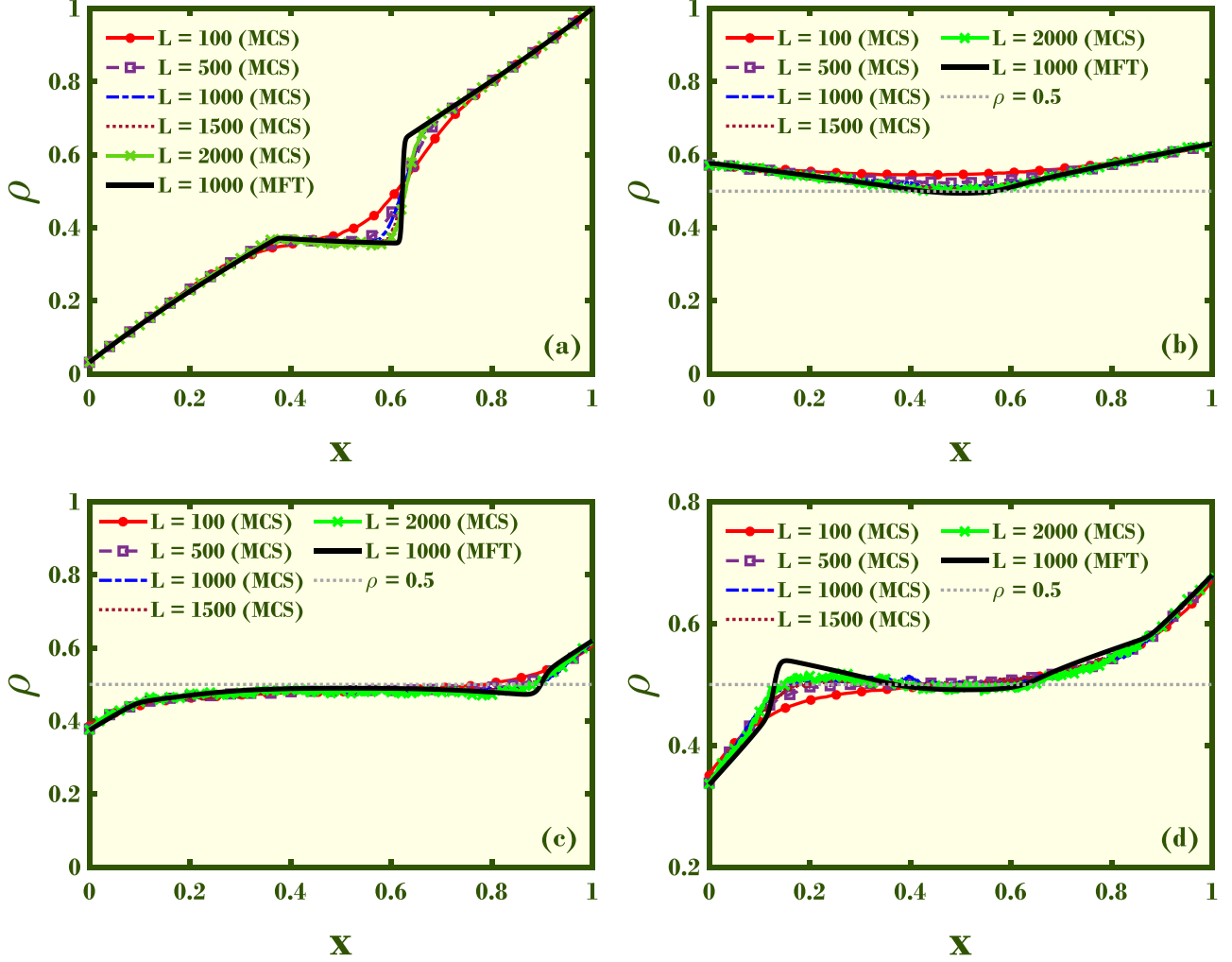


FIG. 7. Finite size effect on shock profile for $\frac{N_r}{L} = 1.4$, (a) $\alpha = 0.1$, $\gamma = 1$, and for $\frac{N_r}{L} = 25$, (b) $\alpha = 0.6$, $\gamma = 0.63$; (c) $\alpha = 0.39$, $\gamma = 0.62$; and (d) $\alpha = 0.35$, $\gamma = 0.68$. The other parameter values of attachment, detachment, and coupling rates are fixed as $\Omega_a = \Omega_d = 0.1$ and $\Omega = 1$, respectively.

system. Beyond the value of $e_4 > 40$, no vital changes are exhibited in the phase diagram except the minor phase boundary shifting. It is noteworthy to mention that the phase diagram contains exactly four distinct steady phases when $\frac{N_r}{L} > 29$, as shown in Fig. 4(c). Besides, beyond the values of the coupling rate 100, except for the phase boundary shifting, the topology of the phase diagram remains the same for the case of $\Omega = 10$ until it reaches the critical value 25. Besides enhancing the value of the number of particles in the system, $\frac{N_r}{L}$, after crossing this critical point, the LD phase evolves into the mixed phase LD/MC/LD. Beyond the value of $\frac{N_r}{L} > 25$, the phase diagram accumulates only three phases, LD/MC/LD, MC, and HD/MC/HD.

From the above discussion, we observe that only for the case of coupling rate $\Omega = 1$ the number of phases changes nonmonotonically in the phase diagram while increasing the value of $\frac{N_r}{L}$ (see Fig. 4). Further, the phase diagram becomes complex and accumulates more phases for different values of the number of particles in the system compared to the phase diagram for all other magnitudes of lane-shifting rate. The reason is that for a comparatively smaller value of coupling rate Ω , there is a greater chance of particles staying in the

lanes, which increases the possibility of competition between the lanes and reservoir.

B. Density profiles and phase transition

The theoretical findings of the system properties, employing the generalized mean-field theory, are verified through Monte Carlo simulation. We obtain the simulation results for 10^{10} – 10^{11} time steps with the lattice size $L = 1000$. From the calculated results, the first 5% of results are ignored to obtain the results in a steady state. We have evaluated the average densities of the lanes by taking the time average over an interval of $10N$. The phase boundaries are determined within an estimated inaccuracy of less than 1%.

We have scrutinized the steady-state properties of the proposed model on account of overall particles in the system and different lane-changing rates. To understand how particles behave along lattices in steady state, a few important distinct density profiles are shown in Fig. 5 as follows: LD [Fig. 5(a)], S [Fig. 5(b)], \tilde{D} [Fig. 5(c)], HD/S [Fig. 5(d)], HD [Fig. 5(e)] for the case of $\frac{N_r}{L} = 3.5$ and HD/LD/HD [Fig. 5(f)], S/LD/HD [Fig. 5(g)], and LD/HD [Fig. 5(h)]

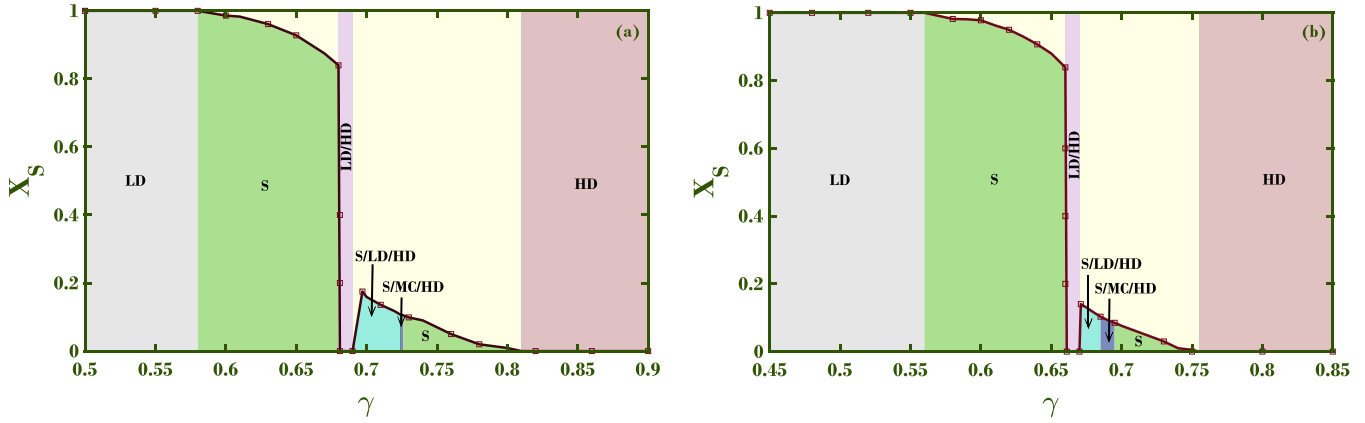


FIG. 8. Shock position (X_s) for the cases of (a) $\frac{N_T}{L} = 9.5$ with the entry rate $\alpha = 0.4$ and (b) $\frac{N_T}{L} = 25$ with the entry rate $\alpha = 0.35$. The LK and coupling rate are kept as $\Omega_a = \Omega_d = 0.1$ and $\Omega = 1$ with the system size $L = 1000$. The solid line (markers) indicate the obtained outcomes from MFT (MCS).

for the case of $\frac{N_T}{L} = 9.5$ with $\Omega = 1$. It is evident that the theoretical findings are in good agreement with the simulation results. Besides, the proposed model results in a few mixed stationary phases, including the unique double shock owing to the companionship of the finite reservoir, LK, and lane-shifting scenarios. In Fig. 6, we have shown the two different types of phase transitions in which we discuss how the \tilde{D} phase appears and disappears while traveling in either vertical or horizontal directions in the phase diagram. In Fig. 6(a), we have shown the different phase transition of lane A from $LD \rightarrow S \rightarrow \tilde{D} \rightarrow HD/S$ for the case of $\frac{N_T}{L} = 2$ with fixed values of $\Omega = 1$ and $\gamma = 0.7$ with varied α . From Fig. 3(b), it is clear that while traveling horizontally through the phase diagram for fixed $\gamma = 0.7$ and varying the value of α from 0 to 1, the above-mentioned phase transitions occur in the phase diagram. First, the system is in the state of LD, and further moving forward via increasing the value of α , the LD state becomes S phase. In addition, at some stage, the S phase develops into a double shock profile owing to the increment of particle entry rate and finally \tilde{D} transits into the mixed phase HD/S. Physically, the origin of double shock can be understood as follows. For $\alpha = 0.3$, due to less supply of particles, a system in the state of LD phase transits into the shock phase near the right end with $\alpha = 0.5$. At this stage, when we further increase the entry rate from 0.5 to 0.7, due to a traffic jam on the lattice rather than moving forward, new particles start accumulating near the left end, creating another traffic-jam-like situation resulting in a second shock near the left end, thereby producing double shock. In addition, we have shown one more phase transition of lane A in Fig. 6(b), where the phase transitions from $LD \rightarrow S \rightarrow \tilde{D} \rightarrow S \rightarrow HD$ for the case of $\frac{N_T}{L} = 3.5$ with fixed entry rate $\alpha = 0.45$, coupling rate $\Omega = 1$, and varied γ . From the figure, it is evident that onset lane density is in the state of LD, and further increasing the value of γ , LD transits to the S phase. Afterward, the single shock phase modifies to the double shock phase, and later \tilde{D} transits to the S phase, which leads to the remarkable characterization of the reentrance transition of the S phase in the phase diagram. At this stage [Fig. 3(c)], one can travel from the S phase to the S phase again through \tilde{D} just by

varying γ with all remaining parameters fixed. In literature, this kind of phase transition is rare and is called reentrance transition. From Fig. 3(c), it is understood that the reentrance effect leads to partial phase division of the shock phase in the phase diagram as the \tilde{D} region resides inside the region of the S phase. Besides advancing the value of γ , finally, the shock phase transits to the HD phase owing to less possibility of particle discharge rate from the lanes.

C. Shock dynamics

The steady-state properties of the proposed model exhibit more fascinating phenomena in phase diagrams due to the reentrance transition and partial phase division of the shock phase, which motivates us to analyze the influence of the lattice size on the shock profile. We have displayed the impact of lattice size on the shock phase with $\alpha = 0.1$ and $\gamma = 1$. The total number of particles in the system is kept as $\frac{N_T}{L} = 1.4$. From Fig. 7(a), it is comprehended that the vertical sharpness of the shock profile increases while increasing the size of the lattice, confirming that the system size does not affect the properties of the system. We have also displayed density profiles of narrow region phases with $\frac{N_T}{L} = 25$ for different values of the lattice size in Figs. 7(b)–7(d). The figure shows that the captured narrow region phases do not vanish in the thermodynamic limit.

Further, we have discussed the nature of shock dynamics by examining the shock location and how the shock phase transits into some other phases while traveling in either a horizontal or vertical direction in the phase diagram. Additionally, one can find out the shock position (x_s) of the lane by employing the steadiness behavior of the current across the shock profile as both the left- and right-hand-side currents of the lane are equal at x_s , as follows:

$$\rho_{j,-}^2 - \rho_{j,-} = \rho_{j,+}^2 - \rho_{j,+}, \tag{20}$$

where $j = A, B$, and

$$\begin{aligned} \rho_{j,-} &= \lim_{x \rightarrow x_s^-} \rho_j(x), \\ \rho_{j,+} &= \lim_{x \rightarrow x_s^+} \rho_j(x). \end{aligned}$$

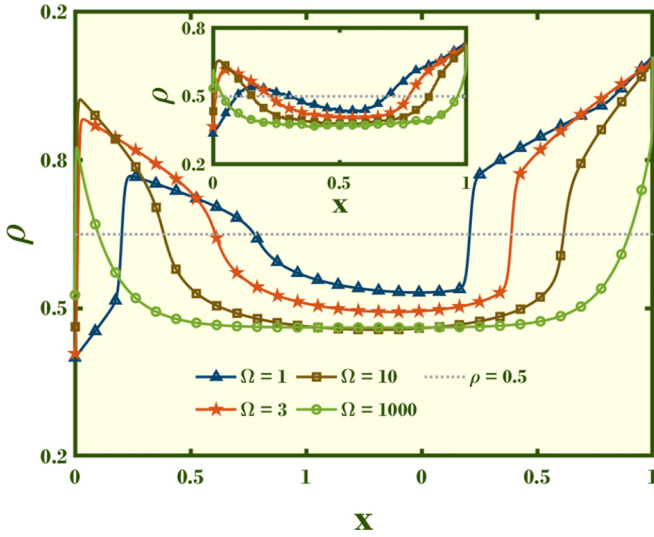


FIG. 9. The impact of coupling rate on the double shock phase for $\frac{N_T}{L} = 2$. The other parameter rates are fixed as $\alpha = 0.7$, $\gamma = 0.74$, $\Omega_a = \Omega_d = 0.1$, and $L = 1000$. The main panel (inset) indicates the MFT (MCS) results.

One can find the implicit form of shock positions in either lane using the above equations. In this direction, Fig. 8(a) highlights the shock position in lane A for $\frac{N_T}{L} = 9.5$ with the fixed rate $\alpha = 0.4$, $\Omega = 1$, and varied rate of γ . For $\gamma = 0.5$, the system is in the LD phase [see Fig. 3(d)], in which the position of the shock is 1. Beyond $\gamma = 0.58$, the single shock phase persists and travels through the left boundary until it reaches 0.68. At $\gamma = 0.68$, the S phase transits to LD/HD where the shock position is zero, lasting until $\gamma = 0.69$. With further increasing the value of γ , the LD/HD phase transits to the mixed-type shock phase S/LD/HD, and this phase transits to S/MC/HD for the tiny interval of γ . Further, advancing γ , the mixed shock phase changes to the S phase, which results in the reentrance transition and partial phase division, and it persists up to $\gamma = 0.81$. Later, the shock phase transits to the HD phase due to the lesser possibility of particle exit from the lane, so the shock position is zero in the high-density state. In the same way, we have displayed one more graph of shock position in Fig. 8(b) in which the total number of available particles in the system is maintained as $\frac{N_T}{L} = 25$ and the entrance and coupling rate are fixed as $\alpha = 0.35$ and $\Omega = 1$ concerning γ .

Moreover, the proposed coupled model also leads to an interesting double shock in the phase diagram. Physically the double shock profile represents two different traffic jams on the lattice. From Fig. 4, it is clear that the double shock exists only for the lower order of lane-changing rate such as $\Omega = 1$. Figure 9 shows how the double shock phase reacts to varying coupling rates. For $\Omega = 1$, we observe that the system experiences the double shock, which transits into HD/S with $\Omega = 3$. With further increase in coupling rate, HD/S transits into HD/LD/HD at $\Omega = 10$. Finally, for $\Omega = 1000$, we obtain a simple LD phase. The influence of coupling rate on double shock can be explained as follows. With an increase in coupling rate, comparatively more particles can jump to another lane, making space for movement

for new particles on the lane leading to the transition of the shock phase into other smooth phases leading to the transitions shown in Fig. 9. Therefore, with higher lane switching, we do not obtain the double shock as particles have the opportunity to go on another lane rather than accumulating on the same lane and creating traffic-jam-like scenarios.

V. CONCLUSION

In this work, we have examined the symmetrically coupled two-lane bidirectional totally asymmetric simple exclusion process with Langmuir kinetics in the presence of limited resources. Instinctively, the proposed model is impelled by vehicular traffic phenomena, where the particles' dynamics in the transport process rely on the finite availability of particles in their surroundings. The influence of limited particles on the system has been investigated for varied values of the total number of particles in the system with various values of coupling rates. The theoretical results are obtained utilizing the generalized mean-field theory, and the derived findings are well matched with the Monte Carlo simulation results. Besides, from the inspection of the topology of the phase diagram for increasing values of $\frac{N_T}{L}$, the critical points concerning coupling rates are found where the phases either appear or disappear or transit into other stationary phases in the phase plane of (α, γ) . In addition, system properties are explained through characteristics including phase diagrams, density profiles, phase transitions, finite size effect, and shock position. The investigation of steady-state properties of the system reveals 15 distinct stationary phases, including the mixed phases LD/HD, S/LD/HD, S/MC/HD, HD/MC/HD, and the unique double shock \bar{D} , which have not been reported in any past studies of TASEP with the involving finite pool.

Moreover, for the smaller values of lane-switching rate, the finite resources affect the system dynamics crucially as the same produces various exciting features, including double shock, even for small values of $\frac{N_T}{L}$, which persists for its intermediate values too. The presence of double shock leads to an exciting reentrance transition where one can travel from one phase to the same phase via other different phases just by varying the entry or exit rate with the remaining parameters fixed. In this study, one can travel from the S phase to the same S phase via the double shock phase just by varying the particular value of α and keeping all other parameters fixed. The exciting finding is that the shape of phase boundaries is peculiar, so even if we vary γ , we can travel from S to S by fixing all other parameters. Therefore, the reentrance transition takes place in two directions, which is very rare and has not been reported in the literature. Apart from these transitions, we also detected one more reentrance transition of a single shock phase where one can move from the S phase to the same S phase through three different mixed phases, LD/HD, S/LD/HD, and S/MC/HD. The existence of the different ways of reentrance transition of the S phase in the same phase diagram leads us to refer to this scenario as a multiple reentrance transition. Moreover, we also observe that phase segregation of the S phase appears in the phase diagram due to the multiple reentrance transition and the presence of double shock and various mixed phases. It is found that while increasing the value of $\frac{N_T}{L}$,

the number of stationary phases in the phase diagram changes nonmonotonically.

For the intermediate values of the lane-shifting rate, the system experiences a total of 12 types of stationary phases in the range $\frac{N_r}{L} \in [0, \infty)$. Here, the number of emerging steady phases in the phase diagram monotonically increases while raising the available number of particles in the reservoir. Besides, at a higher value of $\frac{N_r}{L}$, the system behaves like a symmetrically coupled bidirectional TASEP with LK under the presence of an infinite reservoir. For moderate values of the coupling rate, the system produces five distinct stationary phases, including the three mixed phases for the various values of the total number of particles in the system. Also, it has been observed that the topology of the phase diagram is not affected significantly beyond the higher value of $\frac{N_r}{L}$. Further, we have investigated the structure of the shock profile for different values of system size, so it is established that the lattice size does not affect the system properties dramatically. The lack of finite size effect reveals that the discussed aspects of the system hold for any value of the lattice size. Moreover,

we have discussed various kinds of phase transitions. We examined the shock position to understand the crucial aspects of the reentrance transition and phase segregation phenomena of the shock phase more clearly. From the study, it is clear that the infrastructure of the phase diagram of the system becomes complex while increasing the value of $\frac{N_r}{L}$.

The present study provides insights to understand the complex dynamics of the bidirectional symmetrically coupled traffic phenomenon under the influence of a finite pool of particles. It produces a few exciting features which are not reported in past studies on the incorporation of limited reservoir TASEP models. In the future, this study can be extended to a more general model by including asymmetric coupling rules, bottlenecks, dynamic lattices, etc.

ACKNOWLEDGMENT

A.K.V. acknowledges the support from NIT Trichy, India (Grant No. NITT/R&C/SEED GRANT/2021-2022/PROJ.NO.32).

-
- [1] C. T. MacDonald, J. H. Gibbs, and A. C. Pipkin, Kinetics of biopolymerization on nucleic acid templates, *Biopolymers* **6**, 1 (1968).
 - [2] D. Chowdhury, V. Guttal, K. Nishinari, and A. Schadschneider, A cellular-automata model of flow in ant trails: Non-monotonic variation of speed with density, *J. Phys. A: Math. Gen.* **35**, L573 (2002).
 - [3] S. Klumpp and R. Lipowsky, Traffic of molecular motors through tube-like compartments, *J. Stat. Phys.* **113**, 233 (2003).
 - [4] K. Nagel, Particle hopping models and traffic flow theory, *Phys. Rev. E* **53**, 4655 (1996).
 - [5] D. Chowdhury, L. Santen, and A. Schadschneider, Statistical physics of vehicular traffic and some related systems, *Phys. Rep.* **329**, 199 (2000).
 - [6] L. B. Shaw, R. K. P. Zia, and K. H. Lee, Totally asymmetric exclusion process with extended objects: A model for protein synthesis, *Phys. Rev. E* **68**, 021910 (2003).
 - [7] R. K. P. Zia, J. J. Dong, and B. Schmittmann, Modeling translation in protein synthesis with TASEP: A tutorial and recent developments, *J. Stat. Phys.* **144**, 405 (2011).
 - [8] Y.-Q. Wang, R. Jiang, A. B. Kolomeisky, and M.-B. Hu, Bulk induced phase transition in driven diffusive systems, *Sci. Rep.* **4**, 5459 (2014).
 - [9] A. Parmeggiani, T. Franosch, and E. Frey, Phase Coexistence in Driven One-Dimensional Transport, *Phys. Rev. Lett.* **90**, 086601 (2003).
 - [10] J. Krug, Boundary-Induced Phase Transitions in Driven Diffusive Systems, *Phys. Rev. Lett.* **67**, 1882 (1991).
 - [11] M. R. Evans, D. P. Foster, C. Godrèche, and D. Mukamel, Asymmetric exclusion model with two species: Spontaneous symmetry breaking, *J. Stat. Phys.* **80**, 69 (1995).
 - [12] A. B. Kolomeisky, G. M. Schütz, E. B. Kolomeisky, and J. P. Straley, Phase diagram of one-dimensional driven lattice gases with open boundaries, *J. Phys. A: Math. Gen.* **31**, 6911 (1998).
 - [13] J. Krug, Phase separation in disordered exclusion models, *Braz. J. Phys.* **30**, 97 (2000).
 - [14] A. Goswami, M. Chatterjee, and S. Mukherjee, Steady states and phase transitions in heterogeneous asymmetric exclusion processes, *J. Stat. Mech.* (2022) 123209.
 - [15] N. Sarkar and A. Basu, Nonequilibrium steady states in asymmetric exclusion processes on a ring with bottlenecks, *Phys. Rev. E* **90**, 022109 (2014).
 - [16] P. Roy, A. K. Chandra, and A. Basu, Pinned or moving: States of a single shock in a ring, *Phys. Rev. E* **102**, 012105 (2020).
 - [17] J. Howard, Mechanics of motor proteins, in *Physics of Biomolecules and Cells (Physique des biomolécules et des cellules)*, edited by F. Flyvbjerg, F. Jülicher, P. Ormos, and F. David (Springer, Berlin, 2002), pp. 69–94.
 - [18] M. R. Evans, R. Juhász, and L. Santen, Shock formation in an exclusion process with creation and annihilation, *Phys. Rev. E* **68**, 026117 (2003).
 - [19] A. Parmeggiani, T. Franosch, and E. Frey, Totally asymmetric simple exclusion process with Langmuir kinetics, *Phys. Rev. E* **70**, 046101 (2004).
 - [20] E. Pronina and A. B. Kolomeisky, Two-channel totally asymmetric simple exclusion processes, *J. Phys. A: Math. Gen.* **37**, 9907 (2004).
 - [21] E. Pronina and A. B. Kolomeisky, Asymmetric coupling in two-channel simple exclusion processes, *Physica A* **372**, 12 (2006).
 - [22] R. Jiang, R. Wang, and Q.-S. Wu, Two-lane totally asymmetric exclusion processes with particle creation and annihilation, *Physica A* **375**, 247 (2007).
 - [23] A. K. Gupta and I. Dhiman, Asymmetric coupling in two-lane simple exclusion processes with Langmuir kinetics: Phase diagrams and boundary layers, *Phys. Rev. E* **89**, 022131 (2014).
 - [24] A. K. Verma, A. K. Gupta, and I. Dhiman, Phase diagrams of three-lane asymmetrically coupled exclusion process with Langmuir kinetics, *Europhys. Lett.* **112**, 30008 (2015).

- [25] T. L. Blasius, N. Reed, B. M. Slepchenko, and K. J. Verhey, Recycling of kinesin-1 motors by diffusion after transport, *PLoS One* **8**, e76081 (2013).
- [26] L. Ciandrini, I. Neri, J. Charles Walter, O. Dauloudet, and A. Parmeggiani, Motor protein traffic regulation by supply-demand balance of resources, *Phys. Biol.* **11**, 056006 (2014).
- [27] M. Ha and M. Den Nijs, Macroscopic car condensation in a parking garage, *Phys. Rev. E* **66**, 036118 (2002).
- [28] D. A. Adams, B. Schmittmann, and R. K. P. Zia, Far-from-equilibrium transport with constrained resources, *J. Stat. Mech.* (2008) P06009.
- [29] L. J. Cook and R. K. P. Zia, Feedback and fluctuations in a totally asymmetric simple exclusion process with finite resources, *J. Stat. Mech.* (2009) P02012.
- [30] L. J. Cook, R. K. P. Zia, and B. Schmittmann, Competition between multiple totally asymmetric simple exclusion processes for a finite pool of resources, *Phys. Rev. E* **80**, 031142 (2009).
- [31] P. Greulich, L. Ciandrini, R. J. Allen, and M. C. Romano, Mixed population of competing totally asymmetric simple exclusion processes with a shared reservoir of particles, *Phys. Rev. E* **85**, 011142 (2012).
- [32] A. K. Verma and A. K. Gupta, Limited resources in multi-lane stochastic transport system, *J. Phys. Commun.* **2**, 045020 (2018).
- [33] A. K. Verma, N. Sharma, and A. K. Gupta, Far-from-equilibrium bidirectional transport system with constrained entrances competing for pool of limited resources, *Phys. Rev. E* **97**, 022105 (2018).
- [34] A. Haldar, P. Roy, and A. Basu, Asymmetric exclusion processes with fixed resources: Reservoir crowding and steady states, *Phys. Rev. E* **104**, 034106 (2021).
- [35] B. Pal and A. K. Gupta, Reservoir crowding in a totally asymmetric simple exclusion process with Langmuir kinetics, *Chaos, Solitons Fractals* **153**, 111517 (2021).
- [36] H.-S. Kuan and M. D. Betterton, Motor protein accumulation on antiparallel microtubule overlaps, *Biophys. J.* **110**, 2034 (2016).
- [37] H.-S. Kuan and M. D. Betterton, Phase-plane analysis of the totally asymmetric simple exclusion process with binding kinetics and switching between antiparallel lanes, *Phys. Rev. E* **94**, 022419 (2016).
- [38] S. Tamizhazhagan and A. K. Verma, Role of extended coupling in bidirectional transport system, *Phys. Rev. E* **106**, 014120 (2022).
- [39] C. A. Brackley, L. Ciandrini, and M. C. Romano, Multiple phase transitions in a system of exclusion processes with limited reservoirs of particles and fuel carriers, *J. Stat. Mech.* (2012) P03002.
- [40] A. K. Verma and A. K. Gupta, Stochastic transport on flexible lattice under limited resources, *J. Stat. Mech.* (2019) 103210.
- [41] T. Banerjee and A. Basu, Smooth or shock: Universality in closed inhomogeneous driven single file motions, *Phys. Rev. Res.* **2**, 013025 (2020).
- [42] N. Bhatia and A. K. Gupta, Far from equilibrium transport on TASEP with pockets, *Eur. Phys. J. Plus* **137**, 892 (2022).
- [43] L. J. Cook and R. K. P. Zia, Competition for finite resources, *J. Stat. Mech.* (2012) P05008.